A FOURTH-ORDER RUNGE-KUTTA METHOD WITH EIGHTH-ORDER ACCURACY AND LOW NUMERICAL DISPERSION FOR SOLVING THE SEISMIC WAVE EQUATION

CHAOYUAN ZHANG[1] and LI CHEN[2]

[1] *College of Mathematics and computer, Dali University, Dali 671003, P.R. China. zcy_km@163.com*
[2] *College of Engineering, Dali University, Dali 671003, P.R. China.*

(Received July 19, 2015; revised version accepted January 27, 2016)

ABSTRACT

Zhang, C. and Chen, L., 2016. A fourth-order Runge-Kutta method with eighth-order accuracy and low numerical dispersion for solving the seismic wave equation. *Journal of Seismic Exploration*, 25: 229-255.

In this paper, we give a fourth-order Runge-Kutta method with the eighth-order accuracy and low numerical dispersion for solving the seismic wave equation, which is called the ENAD-FRK method in brief. We first give the theoretical deduction and stability conditions for this new method in detail. And, we derive numerical dispersion relations of the ENAD-FRK method in 2D acoustic case and compare numerical dispersions against the eighth-order Lax-Wendroff correction (LWC) scheme and the eighth-order Staggered-grid (SG) finite difference method. Meanwhile, we compare the memory requirement and the computational efficiency of the proposed method against the eighth-order LWC scheme for modeling 2D seismic wave fields in a two-layer heterogeneous acoustic medium. Last, we apply the ENAD-FRK method to simulate 2D seismic wave propagating in a three-layer homogenous transversely isotropic elastic medium, a two-layer homogenous isotropic elastic medium and a Marmousi model. Simulation results indicate that the ENAD-FRK method can greatly save both computational costs and storage space as contrasted to the eighth-order LWC scheme. Meanwhile, Both comparisons of numerical dispersion analysis and numerical experimental results show that the ENAD-FRK method can effectively suppress numerical dispersion caused by discretizing the seismic wave equation when too coarse grids are used against the eighth-order LWC scheme and the eighth-order SG method.

KEY WORDS: Runge-Kutta method, NAD operator, seismic wave equation, numerical dispersion, wave simulation.

0963-0651/16/$5.00

INTRODUCTION

Numerical methods for solving seismic wave equations and simulating seismic wavefield propagations have played an important role in seismology exploration. Therefore, it becomes very important to develop a more efficient and more accurate numerical simulation method for solving seismic wave propagation equations. As we all know, the finite difference (FD) scheme (Dablain, 1986; Dong et al., 2000; Kelly, 1976; Moczo et al., 2000, 2002) is the most widely used numerical method for solving wave propagation equations in seismology at present. The Lax-Wendroff correction (LWC) scheme (Blanch and Robertsson, 1997; Lax and Wendroff, 1964) and the Staggered-grid (SG)

spatial derivatives included in the converted ODEs. Then, we derive stability conditions for this new method in detail. Meanwhile, we deduce numerical dispersion relations of the ENAD-FRK method in the 2D acoustic case and compare the numerical dispersion against the eighth-order LWC scheme and the eighth-order SG method. Last, we apply the ENAD-FRK method to simulate 2D seismic wave propagating in a two-layered heterogeneous acoustic medium, a three-layered homogenous transversely isotropic elastic medium, a two-layered homogenous isotropic elastic medium and a Marmousi model. Numerical simulation results show that the ENAD-FRK method can significantly reduce numerical dispersion and greatly enhance simulation accuracy. It indicates that the ENAD-FRK method can be used to simulate seismic wave-fields propagating in complex medium and has great potentiality of application in seismology exploration.

THEORY OF THE ENAD-FRK METHOD

The fourth-order Runge-Kutta method for solving ODE

Consider the following ordinary differential equation

$$du/dt = L(u) \quad , \tag{1}$$

where $u = u(x,t)$, with $x \in R^2$ denoting the space variable and t denoting the time variable, and $L(u)$ is a known function with respect to u. We can numerically solve eq. (1) as an ordinary equation using the following fourth-order Runge-Kutta method (Chen et al., 2010)

$$\begin{cases} u^{(1)} = u'' + \frac{1}{2}\Delta t L(u'') \quad , \\ u^{(2)} = u'' + \frac{1}{2}\Delta t L(u^{(1)}) \quad , \\ u^{(3)} = u'' + \Delta t L(u^{(2)}) \quad , \\ u^{n+1} = \frac{1}{3}(-u'' + u^{(1)} + 2u^{(2)} + u^{(3)}) + (1/6)\Delta t L(u^{(3)}) \quad , \end{cases} \tag{2}$$

where Δt is the time step, $u'' = u(n\Delta t)$, $u^{(1)}$, $u^{(2)}$, and $u^{(3)}$ are intermediate variables.

To save storage space and improve calculation speed, eliminating the intermediate variables of $u^{(1)}$, $u^{(2)}$, and $u^{(3)}$ in scheme (2), we can obtain the computational equations as follows

$$\begin{cases} u^* = u'' + \frac{1}{2}\Delta t L(u'') + \frac{1}{4}\Delta t^2 L^2(u'') \quad , \\ u^{n+1} = \frac{1}{3}u'' + \frac{1}{3}\Delta t L(u'') + \frac{2}{3}u^* + \frac{1}{3}\Delta t L(u^*) + (1/6)\Delta t^2 L^2(u^*) \quad , \end{cases} \tag{3}$$

where u* is an intermediate variable, $L^2 = L \cdot L$.

Transformation of wave equations

In 2D anisotropic media, the seismic wave equations describing the elastic wave propagation are given by

$$\rho(\partial^2 u_i/\partial t^2) = (\partial \sigma_{ij}/\partial x_j) + f_i \quad , \quad i = 1,2,3 \tag{4}$$

where the subscript j takes the values of 1 and 3, $\rho = \rho(x,z)$ and σ_{ij} are the density and stress tensor, respectively, u_i and f_i denote the displacement and the force source component in the i-th direction.

Using the stress-strain relations, we transform eq. (4) into the following vector equation

$$\partial^2 U/\partial t^2 = D \cdot U + F \quad , \tag{5}$$

where $U = (u_1,u_2,u_3)^T$, $F = [(1/\rho)f_1,(1/\rho)f_2,(1/\rho)f_3]^T$, and D is the second-order partial differential operator. For examples, for the 2D homogenous isotropic case, D_1 is defined by

$$D_1 = \begin{pmatrix} \dfrac{\lambda+2\mu}{\rho}\dfrac{\partial^2}{\partial x^2} + \dfrac{\mu}{\rho}\dfrac{\partial^2}{\partial z^2} & 0 & \dfrac{\lambda+\mu}{\rho}\dfrac{\partial^2}{\partial x \partial z} \\ 0 & \dfrac{\mu}{\rho}\left(\dfrac{\partial^2}{\partial x^2} + \dfrac{\partial^2}{\partial z^2}\right) & 0 \\ \dfrac{\lambda+\mu}{\rho}\dfrac{\partial^2}{\partial x \partial z} & 0 & \dfrac{\mu}{\rho}\dfrac{\partial^2}{\partial x^2} + \dfrac{\lambda+2\mu}{\rho}\dfrac{\partial^2}{\partial z^2} \end{pmatrix},$$

and for the 2D transverse isotropic case D_2 is defined by

$$D_2 = \begin{pmatrix} \dfrac{c_{11}}{\rho}\dfrac{\partial^2}{\partial x^2} + \dfrac{c_{44}}{\rho}\dfrac{\partial^2}{\partial z^2} & 0 & \dfrac{c_{13}+c_{44}}{\rho}\dfrac{\partial^2}{\partial x \partial z} \\ 0 & \dfrac{c_{66}}{\rho}\dfrac{\partial^2}{\partial z^2} + \dfrac{c_{44}}{\rho}\dfrac{\partial^2}{\partial z^2} & 0 \\ \dfrac{c_{13}+c_{44}}{\rho}\dfrac{\partial^2}{\partial x \partial z} & 0 & \dfrac{c_{44}}{\rho}\dfrac{\partial^2}{\partial x^2} + \dfrac{c_{33}}{\rho}\dfrac{\partial^2}{\partial z^2} \end{pmatrix},$$

where λ, μ, c_{ij} are the elastic constants.

Let $w_i = \partial u_i/\partial t$ (i = 1,2,3) and $W = (w_1,w_2,w_3)^T$. Then eq. (5) can be rewritten as

$$\begin{cases} \partial U/\partial t = W \\ \partial W/\partial t = D\cdot U + F \end{cases} . \tag{6}$$

Let $V = (U,W)^T$, then eq. (6) can be rewritten as follows

$$\partial V/\partial t = L\cdot V + \bar{F} , \tag{7}$$

where L is the differential operator defined by $L = \begin{pmatrix} 0 & I_{3\times 3} \\ D & 0 \end{pmatrix}_{6\times 6}$, and $\bar{F} = (0,F)^T$.

The ENAD-FRK method

Apparently, eq. (7) is a system of ODEs, which can be solved by the idea of solving ODEs. So, we take the following two steps to solve eq. (7).

First, we use the local interpolation method (Yang et al., 2003) to approximate the second- and third-order spatial derivatives of displacement u and particle-velocity w, which are included in the right-hand side of eq. (7), by the linear combinations of u, w, and their spatial gradients at the grid point (i,j) and their neighboring grid points. These computational equations of the eighth-order nearly-analytic discrete operator (Tong et al., 2013; Zhang et al., 2014a,b) for approximating the second- and third-order derivatives are listed in Appendix A for detail.

Second, after the high-order derivatives are discretized, eq. (7) is converted to a system of semi-discrete ODEs with respect to t and can be solved by the four-order Runge-Kutta method [eqs. (3)]. In other words, we can apply eqs. (3) to solve the semi-discrete ODEs (7) as follows

$$\begin{cases} V^* = V^n + \frac{1}{2}\Delta t L(V^n) + \frac{1}{4}\Delta t^2 L^2(V^n) \\ V^{n+1} = \frac{1}{3}V^n + \frac{1}{3}\Delta t L(V^n) + \frac{2}{3}V^n + \frac{1}{3}\Delta t L(V^*) + (1/6)\Delta t^2 L^2(V^*) \end{cases} , \tag{8}$$

where Δt is time step, V^* is intermediate variable, $V^n = V(n\Delta t)$ and $L^2 = L\cdot L$.

Eqs. (8) are called the ENAD-FRK method in brief. Because of using the Taylor series expansion, the errors of $\partial^{m+l}u/\partial x^m \partial z^l$ $(2 \le m+l \le 3)$ are $O(\Delta x^8+\Delta z^8)$ by using the interpolation equations presented in Appendix A. In other words, the ENAD-FRK method is an eighth-order accuracy scheme in space for the 2D case. When the fourth-order Runge-Kutta method is used to solve the Hamiltonian system (7), the temporal derivative error should be $O(\Delta t^4)$. Therefore, the theoretical errors of the ENAD-FRK method are $O(\Delta t^4+\Delta x^8+\Delta z^8)$.

STABILITY CRITERIA

To keep numerical iterations stable, the temporal increment Δt must satisfy the stability condition of the ENAD-FRK method. In the section, we derive the stability conditions of the ENAD-FRK method for 1D and 2D cases. Following the Fourier analysis and the analysis process proposed by Yang et al. (2006), through a series of mathematical operations, we obtain the following stability condition for the 1D homogeneous case (see Appendix B)

$$\Delta t \leq \alpha_{max}(h/c_0) \approx 0.69313(h/c_0) \quad , \tag{9}$$

where $h = \Delta x$ denotes the space increment, α_{max} is the maximum value of the Courant number defined by $\alpha = c_0\Delta t/h$ with the acoustic velocity.

For the 2D homogeneous case, the stability condition of the ENAD-FRK method under the condition $h = \Delta x = \Delta z$ is obtained (Appendix B) and is identical to eq. (9).

As for the elastic case, it is usually complex to derive the exact or analytical stability condition of a numerical scheme for elastic wave equations. When the ENAD-FRK method is applied to solve the 2D elastic wave equation, the stability condition can not be directly determined. But we estimate that the temporal grid size should satisfy the following stability condition

$$\Delta t \leq \Delta t_{max} \approx 0.693(h/c_{max}) \quad , \tag{10}$$

where t_{max} is the maximum temporal increment that keeps the ENAD-FRK method stable for the 2D case, c_{max} is the maximum P-wave velocity, and $h = \Delta x = \Delta z$ is the space increment.

NUMERICAL DISPERSION

In this section, we analyze the numerical dispersion relation of the ENAD-FRK method for the 2D acoustic wave equation (see Appendix C), following those methods proposed in references (Dablain, 1986; Vichnevetsky, 1979; Yang et al., 2012).

Dispersion relations (C-2) and (C-3) show that the numerical dispersion of the ENAD-FRK method is a non-linear function of the propagation angle θ and the Courant number α. Thus we choose wave propagating azimuths of $\theta = 0°, 15°, 30°, 45°$ to investigate the effect of wave propagation directions on the numerical dispersion for the 2D case and compare the ENAD-FRK method against the eighth-order LWC method and the eighth-order SG method.

Fig. 1 shows the variation of numerical dispersion errors along with the sampling ratio S. The abscissa $S = h/\lambda$ denotes the spatial sampling ratio, which shows the ratio of the spatial step h and the wavelength λ. Four curves shown in Fig. 1 denote different propagation directions $\theta = 0°, 15°, 30°, 45°$, respectively. The curves plotted in Figs. 1(a)-(b) are the numerical dispersion ratio of the ENAD-FRK method for the Courant numbers 0.2 and 0.5, respectively. From Figs. 1(a)-(b), we can observe that the ENAD-FRK method has very small numerical dispersion. Figs. 1(c)-(d) and Figs. 1(e)-(f) give the numerical dispersion curves of the eighth-order LWC method and the eighth-order SG method, respectively. Compared with Figs. 1(a)-(b), the numerical dispersion shown in Figs. 1(c)-(f) is more serious.

Table 1 shows that the maximum phase velocity errors of the ENAD-FRK method, the eighth-order LWC method, and the eighth-order SG method for the Courant numbers 0.1, 02, 0.3, 0.4, 0.5, and 0.6. The maximum dispersion error of the ENAD-FRK method is less than 4%, whereas the eighth-order LWC method is about 18.77% and the eighth-order SG method is about 22.96%. Table 2 gives the maximal difference of the numerical dispersion between different propagation directions of the ENAD-FRK method, the eighth-order LWC method, and the eighth-order SG method for the Courant numbers 0.1, 02, 0.3, 0.4, 0.5, and 0.6. The maximal difference of the eighth-order LWC method is about 16.07% and the eighth-order SG method is about 29.41%, while the ENAD-FRK method is less than 2%. This implies that the ENAD-FRK method has very small numerical dispersion and less numerical dispersion anisotropy. In short, the ENAD-FRK method has much less numerical dispersion than the eighth-order LWC and SG methods.

Table 1. The maximum dispersion errors in different wave propagation directions for different methods.

Courant	The ENAD-FRK	The eighth-order LWC	The eighth-order SG
0.1	0.024230	0.187670	0.178835
0.2	0.025160	0.185550	0.171797
0.3	0.028331	0.181909	0.159290
0.4	0.033784	0.176561	0.139844
0.5	0.037653	0.169181	0.110501
0.6	0.027902	0.159197	0.229598

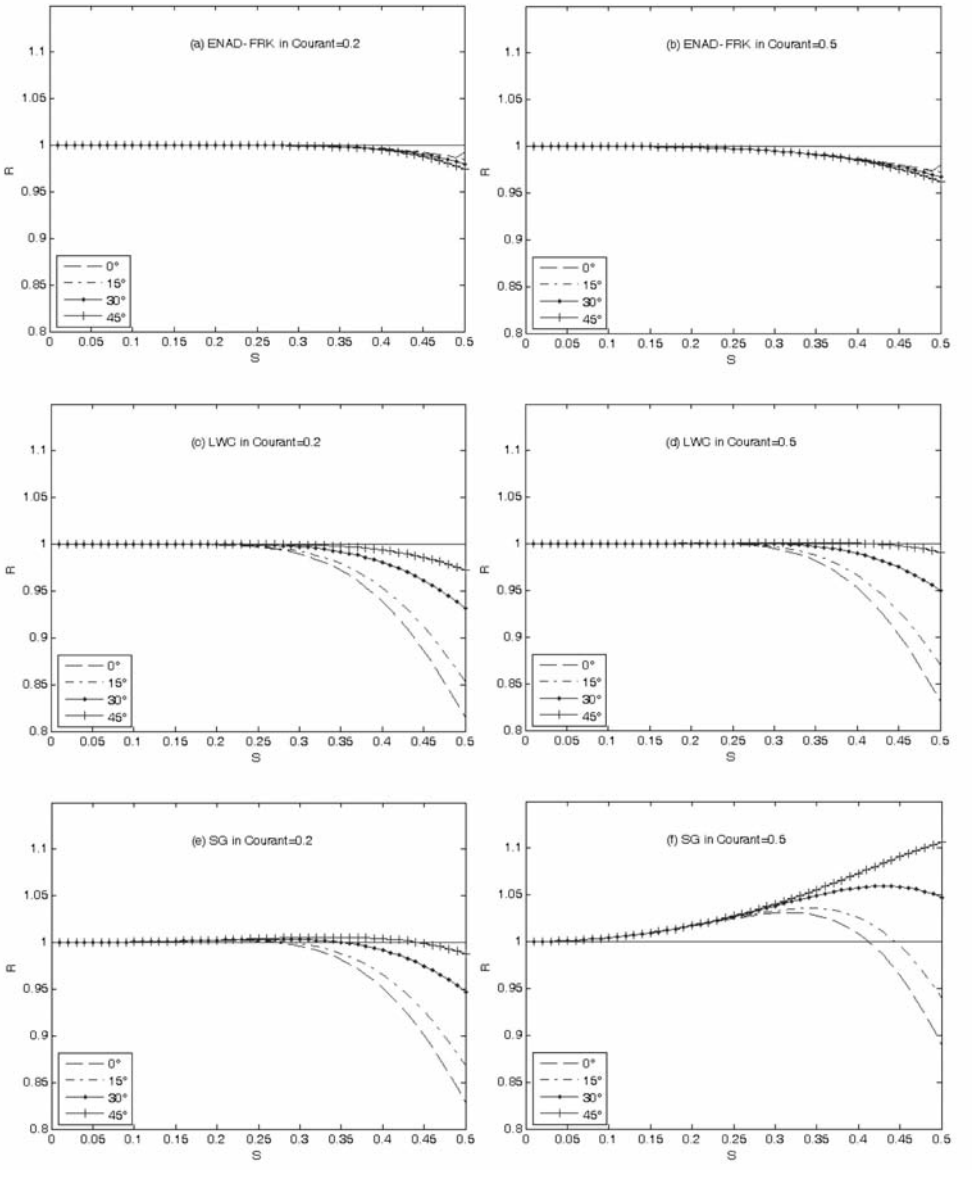

Fig. 1. Numerical dispersion ratios of the ENAD-FRK, the eighth-order LWC, and the eighth-order SG for the Courant numbers 0.2 and 0.5, in four directions of $\theta = 0°$, 15°, 30°, and 45°.

Table 2. The maximum differences of the maximum dispersion errors in different wave propagation directions for different methods.

Courant	The ENAD-FRK	The eighth-order LWC	The eighth-order SG
0.1	0.018076	0.157039	0.154933
0.2	0.017993	0.157563	0.159867
0.3	0.017744	0.158388	0.169268
0.4	0.017472	0.159410	0.185806
0.5	0.017875	0.160390	0.216831
0.6	0.012082	0.160734	0.294144

NUMERICAL EXPERIMENTS

In order to further investigate the computational efficiency and the numerical dispersion of the ENAD-FRK method, we apply this method to simulate 2D seismic wave-fields propagating in a two-layer heterogeneous acoustic medium, a three-layer homogenous transversely isotropic elastic medium, a two-layer homogenous isotropic elastic medium, and a Marmousi model.

Two-layer heterogeneous acoustic model

In our first example, we choose a two-layer heterogeneous acoustic model with varying velocities, which is shown in Fig. 2. The computational domain is $0 \leq x,z \leq 25$ km. The vertical interface is at a depth of 12.5 km. The explosive source with $f_0 = 28$ Hz is at the centre of the computational domain. The spatial increment and time step are $h = \Delta x = \Delta z = 50$ m and $\Delta t = 0.0025$ s, respectively. The source function has the following expression

$$f(t) = -5.76f_0^2[1 - 16(0.6f_0t-1)^2] \times \exp[-8(0.6f_0t-1)^2] \quad . \tag{11}$$

Figs. 3a and 3b show the snapshots at $T = 2.0$ s on the coarse grid of $\Delta x = \Delta z = 50$ m, generated by the ENAD-FRK method and the eighth-order LWC method, respectively. From Figs. 3(a,b), we can observe that the wave-fronts of acoustic waves simulated by these two methods are basically identical, though the computational cost of the ENAD-FRK method is more expensive than the eighth-order LWC method for the same number of grid points because more

variables including displacement, particle-velocity, and their gradients are simultaneously calculated in the ENAD-FRK method. However, the snapshot [see Figs. 3(a)] generated by the ENAD-FRK method has much less numerical dispersion even though the spatial size is 50 m, whereas the eighth-order LWC method suffers from serious numerical dispersion [see Fig. 3(b)]. It indicates that the ENAD-FRK method can be used to simulate large-scale models with coarse grids.

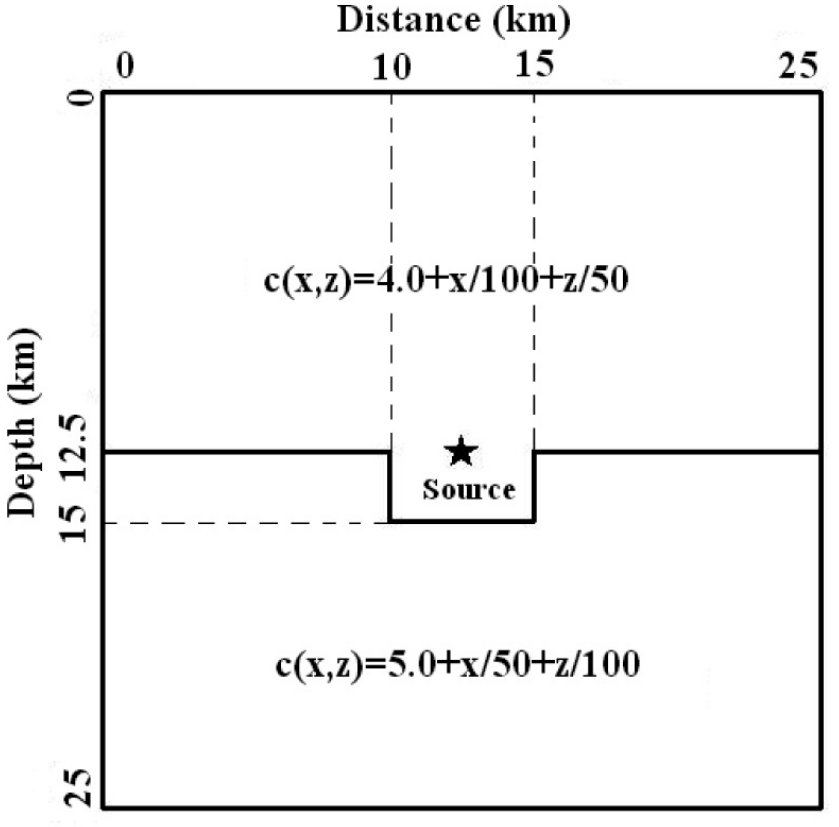

Fig. 2. Two-layer heterogeneous acoustic model with varying velocities.

For exactly eliminating the numerical dispersion, Fig. 3(c) generated by the eighth-order LWC method shows the snapshot at T = 2.0 s under the same Courant number with Figs. 3(a,b) and on a fine grid of $\Delta x = \Delta z = 25$ m, corresponding to the numbers of grid points of 1001×1001. While for the same computational domain, the number of mesh points for the ENAD-FRK method is only 501×501 on the coarse grid of $\Delta x = \Delta z = 50$ m. As a result, the memory requirement of the ENAD-FRK method is approximately 25.05% of that of the eighth-order LWC method.

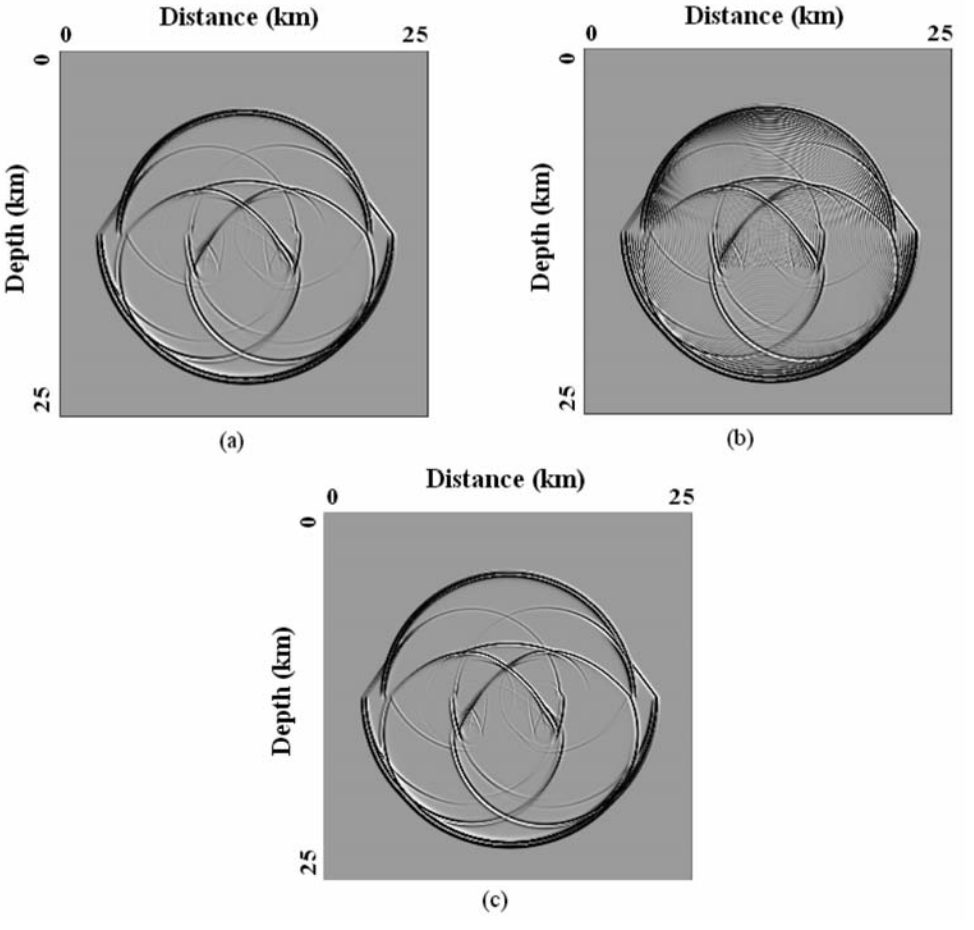

Fig. 3. Snapshots of wave-fields at time 2.0 s, generated by (a) the ENAD-FRK ($\Delta x = \Delta z = 50$ m), (b) the eighth-order LWC ($\Delta x = \Delta z = 50$ m), and (c) the eighth-order LWC ($\Delta x = \Delta z = 25$ m).

Comparison between Fig. 3(a) and Fig. 3(c), demonstrates that our proposed method can provide the same accuracy as the eighth-order LWC method on a fine grid under the same Courant number. But their computational costs are different. It took the ENAD-FRK method about 714 s to generate Fig.3(a), whereas it took the eighth-order LWC method about 1801 s to generate Fig. 3(c). It suggests that the computational efficiency of the ENAD-FRK method is about 2.52 times of that of the eighth-order LWC method on a fine grid to achieve the same accuracy without visible numerical dispersion. Note that our all numerical experiments are performed on a 2-core Pentium-4 computer with 2.33G memory.

Three-layer homogeneous transversely isotropic model

In our second example, we select the elastic wave equations in a 2D homogenous transversely isotropic medium as follows

$$\begin{cases} \rho(\partial^2 u_1/\partial t^2) = c_{11}(\partial^2 u_1/\partial x^2) + c_{44}(\partial^2 u_1/\partial z^2) + (c_{13}+c_{44})(\partial^2 u_3/\partial x \partial z) + f_1 , \\ \rho(\partial^2 u_3/\partial t^2) = (c_{13}+c_{44})(\partial^2 u_1/\partial x \partial z) + c_{44}(\partial^2 u_3/\partial x^2) + c_{33}(\partial^2 u_3/\partial z^2) + f_3 , \end{cases} \tag{12}$$

where u_1,u_3 denote the displacement components in the x- and z-directions, respectively. c_{11}, c_{13}, c_{33} and c_{44} are elastic constants, ρ is the medium density, f_1 and f_3 are the force source components in the x- and z-directions.
In this numerical experiment, we use a three-layer model with parameters of elastic constants and medium densities given in Table 3. The model domain is $0 \leq x,z \leq 12$ km. The explosive source $f_1 = f_3 = f(t)$, of the Ricker wavelet with a frequency of $f_0 = 12$ Hz is located at the centre of the computational domain. The temporal and spatial increments are chosen at $\Delta t = 2$ ms and $\Delta x = \Delta z = 40$ m, respectively. The receivers R1 and R2 are (6 km, 6 km) and (5km, 6km), respectively.

Table 3. Parameters used in a three-layer model.

Layer (No.)	Thickness (km)	c_{11} (GPa)	c_{13} (GPa)	c33 (GPa)	c_{44} (GPa)	ρ (g/cm^3)
1	4.0	45.0	9.6	37.5	12.0	1.0
2	4.0	32.5	7.5	19.5	6.5	2.0
3	4.0	40.8	13.2	50.6	25.0	4.2

Fig. 4, generated by the ENAD-FRK method, shows the snapshots of the x- and z-directions displacement component at time T = 1.2 s. Fig.5, generated by the ENAD-FRK method, shows the wave-fields seismograms of the horizontal displacement component and the vertical displacement component at receivers R1 and R2 from T = 0 to T = 1.2 s. From Figs. 4 and 5, we can see that the ENAD-FRK method shows very clear results and has no visible numerical dispersion. It suggests that the ENAD-FRK method can be efficient to suppress the numerical dispersions and can provide the accurate results for the elastic wave modeling in a three-layer homogeneous transversely isotropic medium of the 2D case.

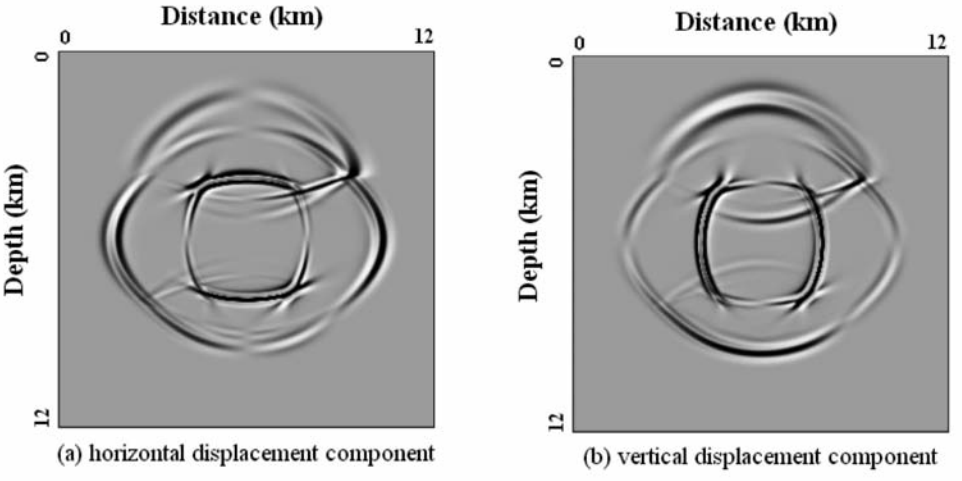

Fig. 4. Snapshots of elastic wave fields at time 1.2 s, generated by the ENAD-FRK method.

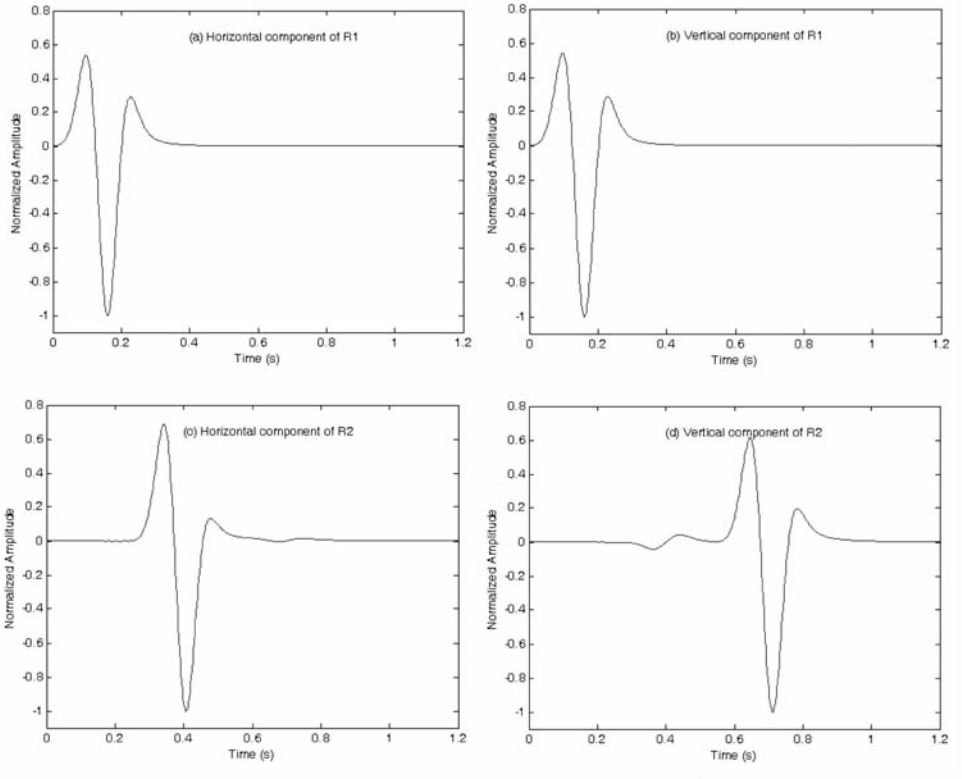

Fig. 5. Elastic wave fields seismograms generated by the ENAD-FRK method.

Two-layer homogeneous isotropic model

In our third example, we choose the elastic wave equations in a 2D homogeneous isotropic medium as follows

$$\begin{cases} \rho(\partial^2 u_1/\partial t^2) = (\lambda+2\mu)(\partial^2 u_1/\partial x^2) + \mu(\partial^2 u_1/\partial z^2) + (\lambda+\mu)(\partial^2 u_3/\partial x \partial z) + f_1, \\ \rho(\partial^2 u_3/\partial t^2) = (\lambda+\mu)(\partial^2 u_1/\partial x \partial z) + \mu(\partial^2 u_3/\partial x^2) + (\lambda+2\mu)(\partial^2 u_3/\partial z^2) + f_3, \end{cases} \tag{13}$$

where u_1, u_3 denote the displacement components in the x- and z-directions, respectively. λ, μ are Lamé parameters, ρ is the medium density, f_1 and f_3 are the force source components in the x- and z-directions.

In this experiment, we simulate the elastic wave [see eq. (13)] propagating through a two-layer homogenous isotropic medium for the 2D case. The size of the computational domain is $0 \leq x,z \leq 9.6$ km and the horizontal interface is at the depth of $z = 3.84$ km. We take the Lamé parameters and densities of $\lambda_1 = 1.12$ GPa, $\mu_1 = 2.592$ GPa and $\rho_1 = 1.8$ g/cm^3 in the upper part, and $\lambda_2 = 7.35$ GPa, $\mu_2 = 13.125$ GPa and $\rho_2 = 2.1$ g/cm^3 in the lower layer, respectively. The explosive source, $f_1 = f_3 = f(t)$, of the Ricker wavelet with a frequency $f_0 = 14$ is located at O(4.8 km, 3.12 km). Spatial and temporal increments are chosen as $\Delta x = \Delta z = 30$ m and $\Delta t = 0.0032$ s.

Fig. 6 shows the snapshots of the x- and z-direction displacement component at time $T = 1.5$ s, generated by the ENAD-FRK method, the eighth-order LWC method, and the eighth-order SG method, respectively. From Fig. 6, we can see that the results of the eighth-order LWC method (c, d) and the eighth-order SG method (e, f) show serious numerical dispersion in the low-velocity layer and at the strong interface, whereas Figs. 6(a,b) generated by the ENAD-FRK method show very clear result and has no visible numerical dispersion even for the large vertical velocity contrast. It demonstrates that the ENAD-FRK method is very effective in suppressing numerical dispersion for simulating the elastic wave propagation through a two-layer homogenous isotropic medium of the 2D case.

Marmousi model

In the last numerical example, the Marmousi model shown in Fig. 7 is chosen to demonstrate the performance of the ENAD-FRK method for the complex heterogeneous case. As shown in Fig. 7, the wave velocity varies from 1.5 km/s to 4.0 km/s. We choose the temporal increment $\Delta t = 0.001$ s and the spatial increment $\Delta x = \Delta z = 24$ m, respectively. The number of mesh points is 384×122. Hence, the computational domain of this model is $0 \leq x \leq 9.192$ km and $0 \leq z \leq 2.904$ km. The source with the frequency $f_0 = 15$ Hz

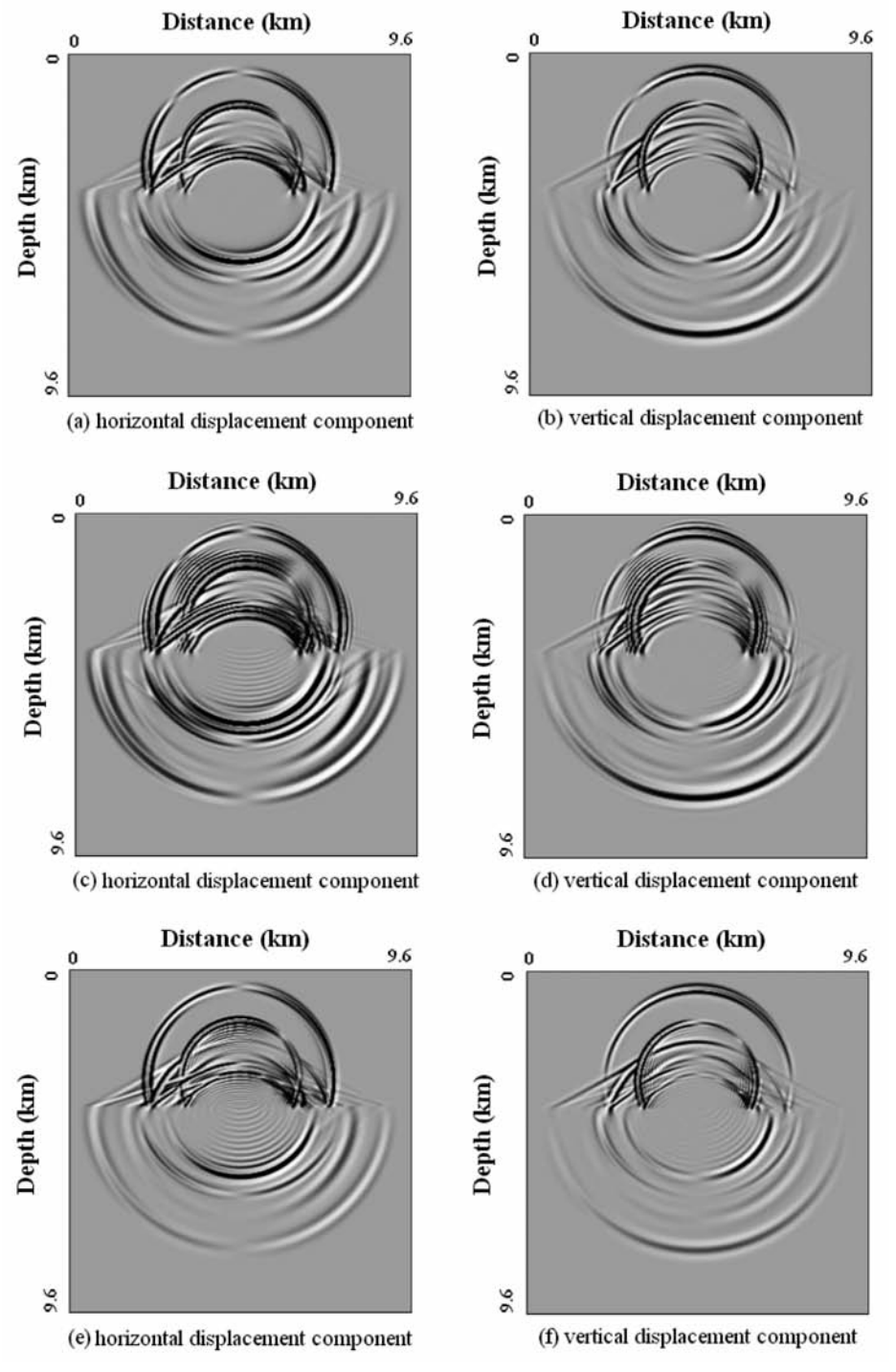

Fig. 6. Snapshots of elastic wave fields for the two-layer model at time 1.5 s, generated by the ENAD-FRK (a, b), the eighth-order LWC (c, d), and the eighth-order SG (e, f), respectively.

is the same as that used in our first model, and is located at (x,z) = (4596 m, 24 m). In this example, the 2-times absorbing boundary condition presented by Yang et al. (2002) is used to eliminate the reflections at the artificial boundaries.

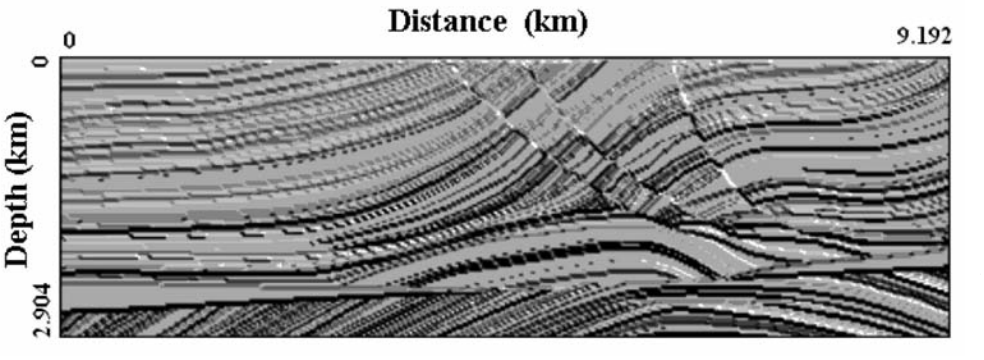

Fig. 7. The Marmousi model (The acoustic velocity varies from 1.5-4.0 km/s).

Fig. 8 displays the wavefield snapshots generated using the ENAD-FRK method at time T = 0.6 s, 0.9 s, 1.2 s and 1.5 s, respectively. In Fig. 8, these snapshots are clean and have no visible numerical dispersion. It illustrates that the ENAD-FRK method can effectively suppress numerical dispersion for the complex heterogeneous case even with a large spatial increment. Meanwhile, this numerical experiment also shows that the ENAD-FRK method has strong adaptability even if the velocity varies from 1.5-4.0 km/s.

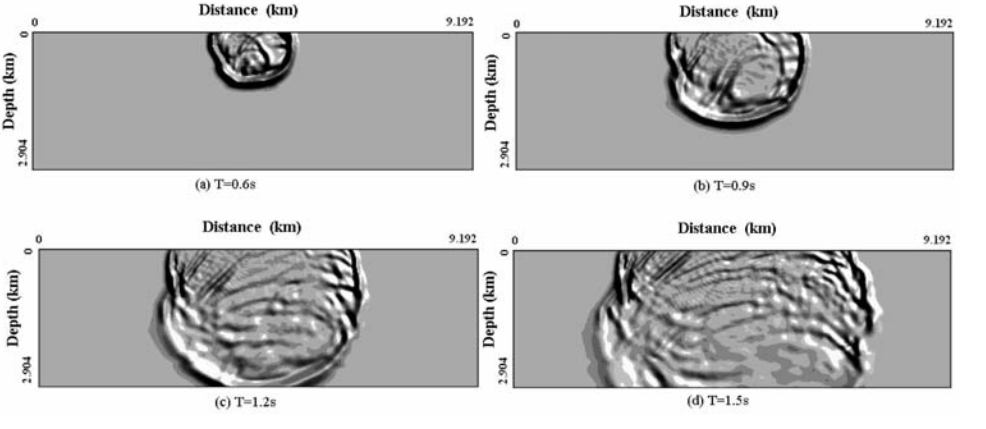

Fig. 8. Snapshots of seismic wave fields for the Marmousi model at a time of T = 0.6 s, 0.9 s, 1.2 s, and 1.5 s, generated using the ENAD-FRK method.

Fig. 9, generated by the ENAD-FRK method, shows a clear waveform on the surface without visible numerical dispersion. The synthetic seismogram is recorded from 384 receivers from x = 0 km to x = 9.192 km with spacing of 24 m on the surface. This numerical result illustrates that it is efficient for the ENAD-FRK method to combine with the 2-times absorbing boundary condition (Yang et al., 2002). This experiment further indicates that the ENAD-FRK method can be used to simulate seismic-wave propagating in complex media.

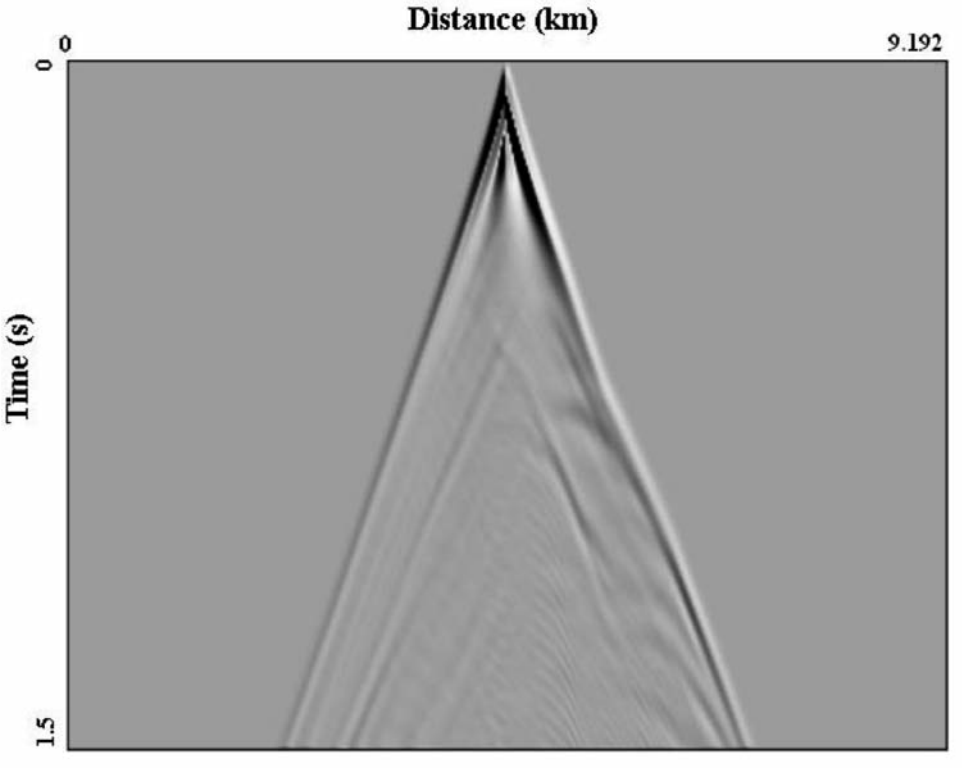

Fig. 9. Synthetic seismogram on the surface for the Marmousi model, generated by the ENAD-FRK method.

CONCLUSIONS AND DISCUSSION

In this paper, we give the ENAD-FRK method with eighth-order accuracy and low numerical dispersion for solving seismic wave equations. The partial differential wave equations are first transformed into a system of ordinary differential equations (ODEs), and then the time derivatives are approximated using the fourth-order Runge-Kutta method, while the space derivatives are calculated using the nearly analytic discrete operator with the eighth-order accuracy. So the ENAD-FRK method is eighth-order accurate in space and

fourth-order accurate in time. Because the approximating equations listed in Appendix A are dependent on values of the displacement and the particle velocity, together with their gradients, the ENAD-FRK method can effectively suppress numerical dispersion using few sampling points per minimum wavelength.

We derive the stability conditions of the ENAD-FRK method for solving 1D and 2D seismic equations (see Appendix B). Meanwhile, we deduce the numerical dispersion relations of the 2D case (see Appendix C) and analyze numerical dispersions. The maximum dispersion error of the ENAD-FRK method is less than 4%, whereas the eighth-order LWC method is about 18.77% and the eighth-order SG method is about 22.96%. The maximal difference of the eighth-order LWC method is about 16.07% and the eighth-order SG method is about 29.41%, while the ENAD-FRK method is less than 2%. This comparison shows that the ENAD-FRK method has very small numerical dispersion and less numerical dispersion anisotropy.

We compare the memory requirement and the computational efficiency of the ENAD-FRK method against the eighth-order LWC scheme for modeling 2D seismic waves fields in a two-layer heterogeneous acoustic medium. The memory requirement of the ENAD-FRK method is approximately 25.05% of that of the eighth-order LWC method and the computational efficiency is about 2.52 times of that of the eighth-order LWC method on a fine grid to achieve the same accuracy without visible numerical dispersion.

Last, we apply the ENAD-FRK method to simulate 2D seismic waves propagating in a three-layer homogenous transversely isotropic elastic medium, a two-layer homogenous isotropic elastic medium and a Marmousi model. All numerical experiments are performed on a 2-core Pentium 4 computer with 2.33G memory.

All numerical examples demonstrate that the ENAD-FRK method is more efficient than the high-order methods such as the eighth-order LWC method and the eighth-order SG method in suppressing the numerical dispersion. Simulation results also show that the ENAD-FRK method has weak numerical dispersion and high computational accuracy. It implies that the ENAD-FRK method can be used to model seismic wave fields propagating in more complex medium and has great potentiality of application in seismic exploration.

ACKNOWLEDGEMENTS

This work was supported by the National Natural Science Foundation of China (Grant Nos. 41464004 and 41230210) and the Science Foundation of the Education Department of Yunnan Province (No.2013Z152).

REFERENCES

Blanch, J.O. and Robertsson, A., 1997. A modified Lax-Wendroff correction for wave propagation in media described by Zener elements. Geophys. J. Internat., 131: 381-386.

Chen, S., Yang, D.H and Deng, X.Y., 2010. An improved algorithm of the fourth-order Runge-Kutta method and seismic wave-field simulation. Chinese J. Geophys. (in Chinese), 3: 1196-1206.

Dablain, M.A., 1986. The application of high-order differencing to scalar wave equation. Geophysics, 51: 54-66.

Dong, L.G., Ma, Z.T., Cao, J.Z., Wang, H.Z., Gong, J.H., Lei, B. and Xu, S.Y., 2000. A staggered-grid high-order difference method of one-order elastic wave equation. Chinese J. Geophys. (in Chinese), 43: 411-419.

Kelly, K.R., Wave, R.W. and Treitel, S., 1976. Synthetic seismograms: a finite-difference approach. Geophysics, 41: 2-27.

Lax, P.D, and Wendroff, B., 1964. Difference schemes for hyperbolic equations with high order of accuracy. Commun. Pure Appl. Mathem., 17: 381-398.

Moczo, P., Kristek, J. and Halada, L., 2000. 3D 4th-order staggered-grid finite-difference schemes: stability and grid dispersion. Bull. Seismol. Soc. Am., 90: 587-603.

Moczo, P., Kristek, J., Vavrŷcuk, V., Archuleta, R.J. and Halada, L., 2002. 3D heterogeneous staggered-grid finite-difference modeling of seismic motion with volume harmonic and arithmetic averaging of elastic moduli and densities. Bull. Seismol. Soc. Am., 92: 3042-3066.

Saenger, E.H., Gold, N. and Shapiro, S.A., 2000. Modeling the propagation of elastic waves using a modified finite-difference grid. Wave Motion, 31: 77-92.

Tong, P., Yang, D.H., Hua, B.L. and Wang, M.X., 2013. A high-order stereo-modeling method for solving wave equations. Bull. Seismol. Soc. Am., 103: 811-833.

Vichnevetsky, R., 1979. Stability charts in the numerical approximation of partial differential equations. a review. Mathemat. Comput. Simul., 21: 170-177.

Virieux, J., 1986. P-SV wave propagation in heterogeneous median: Velocity-stress finite-difference method. Geophysics, 51: 889-901.

Wang, L., Yang, D.H. and Deng, X.Y., 2009. A WNAD method for seismic stress-field modeling in heterogeneous media. Chinese J. Geophys. (in Chinese), 52: 1526-1535.

Yang, D.H., Chen, S. and Li, J.Z., 2007a. A Runge-Kutta method using high-order interpolation approximation for solving 2D acoustic and elastic wave equations. J. Seismic Explor., 16: 331-353.

Yang, D.H., Liu, E., Zhang, Z.J. and Teng, J.W., 2002. Finite-difference modeling in two-dimensional anisotropic media using a flux-corrected transport technique. Geophys. J. Internat., 148: 320-328.

Yang, D.H., Peng, J.M., Lu, M. and Terlaky, T., 2006. Optimal nearly-analytic discrete approximation to the scalar wave equation. Bull. Seismol. Soc. Am., 96: 1114-1130.

Yang, D.H., Song, G.J., Chen, S. and Hou, B.Y., 2007b. An improved nearly analytical discrete method: an efficient tool to simulate the seismic response of 2-D porous structures. J. Geophys. Engin., 4: 40-52.

Yang, D.H., Teng, J.W., Zhang, Z.J. and Liu, E., 2003. A nearly-analytic discrete method for acoustic and elastic wave equations in anisotropic media. Bull. Seismol. Soc. Am., 93: 882-890.

Yang, D.H., Tong, P. and Deng, X.Y., 2012. A central difference method with low numerical dispersion for solving the scalar wave equation. Geophys. Prosp., 60: 885-905.

Yang, D.H., Wang, N., Chen, S. and Song, G.J., 2009. An explicit method based on the implicit Runge-Kutta algorithm for solving the wave equations. Bull. Seismol. Soc. Am., 99: 3340-3354.

Zeng, Y.Q. and Liu, Q.H., 2001. A staggered-grid finite-difference method with perfectly matched layers for poroelastic wave equations. J. Acoust. Soc. Am., 109: 571-2580.

Zhang, C.Y., Li, X., Ma, X. and Song, G.J., 2014a. A Runge-Kutta method with using eighth-order nearly-analytic spatial discretization operator for solving a 2D acoustic wave equation. J. Seismic Explor., 23: 279-302.

Zhang, C.Y., Ma, X., Yang, L. and Song, G.J., 2014b. Symplectic partitioned Runge-Kutta method based on the eighth-order nearly analytic discrete operator and its wavefield simulations. Appl. Geophys., 11: 89-106.

Zhang, Z.J., Wang, G.J. and Harris, J.M., 1999. Multi-component wave-field simulation in viscous extensively dilatancy anisotropic media. Phys. Earth Planet. Inter., 114: 25-38.

Zheng, H.S,, Zhang, Z.J. and Liu, E., 2006. Non-linear seismic wave propagation in anisotropic media using the flux-corrected transport technique. Geophys. J. Internat., 65: 943-956.

APPENDIX A

APPROXIMATION OF EIGHTH-ORDER DERIVATIVES

In order to obtain the approximation equations of eighth-order derivatives in eq. (7), Tong et al. (2013) derived these approximate equations. For convenience, here we present the approximation equations of the displacement as follows:

$$\partial^2 u_{j,k}/\partial x^2 = (1/\Delta x^2)\{(7/54)[u_{j-2,k}+u_{j+2,k}]+(64/27)[u_{j-1,k}+u_{j+1,k}]-5u_{j,k}\}$$

$$+ (1/\Delta x)\{(1/36)[(\partial u_{j-2,k}/\partial x)-(\partial u_{j+2,k}/\partial x)]+(8/9)[(\partial u_{j-1,k}/\partial x)-(\partial u_{j+1,k}/\partial x)]\} , \quad \text{(A-1)}$$

$$\partial^2 u_{j,k}/\partial z^2 = (1/\Delta z^2)\{(7/54)[u_{j,k-2}+u_{j,k+2}]+(64/27)[u_{j,k-1}+u_{j,k+1}]-5u_{j,k}\}$$

$$+ (1/\Delta z)\{(1/36)[(\partial u_{j,k-2}/\partial z)-(\partial u_{j,k+2}/\partial z)]+(8/9)[(\partial u_{j,k-1}/\partial z)-(\partial u_{j,k+1}/\partial z)]\} , \quad \text{(A-2)}$$

$$\partial^2 u_{j,k}/\partial x\partial z = (7/216\Delta x\Delta z)[u_{j-2,k-2} + u_{j+2,k+2} - u_{j-2,k+2} - u_{j+2,k-2}]$$

$$+ (16/27\Delta x\Delta z)[u_{j-1,k-1} + u_{j+1,k+1} - u_{j-1,k+1} - u_{j+1,k-1}]$$

$$+ (1/144\Delta x)[(\partial u_{j-2,k-2}/\partial z)-(\partial u_{j+2,k+2}/\partial z)+(\partial u_{j-2,k+2}/\partial z)-(\partial u_{j+2,k-2}/\partial z)]$$

$$+ (1/144\Delta z)[(\partial u_{j-2,k-2}/\partial x)-(\partial u_{j+2,k+2}/\partial x)+(\partial u_{j+2,k-2}/\partial x)-(\partial u_{j-2,k+2}/\partial x)]$$

$$+ (2/9\Delta x)[(\partial u_{j-1,k-1}/\partial z)-(\partial u_{j+1,k+1}/\partial z)+(\partial u_{j-1,k+1}/\partial z)-(\partial u_{j+1,k-1}/\partial z)]$$

$$+ (2/9\Delta z)[(\partial u_{j-1,k-1}/\partial x)-(\partial u_{j+1,k+1}/\partial x)+(\partial u_{j+1,k-1}/\partial x)-(\partial u_{j-1,k+1}/\partial x)] , \quad \text{(A-3)}$$

$$\partial^3 u_{j,k}/\partial x^3 = (1/\Delta x^3)\{-(31/144)[u_{j-2,k}-u_{j+2,k}]-(88/9)[u_{j-1,k}-u_{j+1,k}]\}$$

$$+ (1/\Delta x^2)\{-(1/24)[(\partial u_{j-2,k}/\partial x)+(\partial u_{j+2,k}/\partial x)]-(8/3)[(\partial u_{j-1,k}/\partial x)+(\partial u_{j+1,k}/\partial x)]$$

$$-15(\partial u_{j,k}/\partial x)\} , \quad \text{(A-4)}$$

$$\partial^3 u_{j,k}/\partial z^3 = (1/\Delta z^3)\{-(31/144)[u_{j,k-2}-u_{j,k+2}]-(88/9)[u_{j,k-1}-u_{j,k+1}]\}$$
$$+ (1/\Delta z^2)\{-(1/24)[(\partial u_{j,k-2}/\partial z)+(\partial u_{j,k+2}/\partial z)]-(8/3)[(\partial u_{j,k-1}/\partial z)+(\partial u_{j,k+1}/\partial z)]$$
$$-15(\partial u_{j,k}/\partial z)\}\ , \qquad \text{(A-5)}$$

$$\partial^3 u_{j,k}/\partial x\partial z^2 = (31/864\Delta x\Delta z^2)[u_{j+2,k+2} - u_{j-2,k-2} + u_{j+2,k-2} - u_{j-2,k+2}$$
$$+ 2u_{j-2,k} - 2u_{j+2,k}]$$
$$+ (44/27\Delta x\Delta z^2)[u_{j+1,k+1} - u_{j-1,k-1} + u_{j+1,k-1} - u_{j-1,k+1} + 2u_{j-1,k}$$
$$- 2u_{j+1,k}]$$
$$- (1/144\Delta z^2)[(\partial u_{j-2,k-2}/\partial x) + (\partial u_{j+2,k+2}/\partial x) + (\partial u_{j-2,k+2}/\partial x)$$
$$+ (\partial u_{j+2,k-2}/\partial x) - 2(\partial u_{j+2,k}/\partial x) - 2(\partial u_{j-2,k}/\partial x)]$$
$$- (4/9\Delta z^2)[(\partial u_{j-1,k-1}/\partial x)+(\partial u_{j+1,k+1}/\partial x)+(\partial u_{j-1,k+1}/\partial x)+(\partial u_{j+1,k-1}/\partial x)$$
$$- 2(\partial u_{j+1,k}/\partial x) - 2(\partial u_{j-1,k}/\partial x)]$$
$$- (1/144\Delta x\Delta z)[(\partial u_{j-2,k-2}/\partial z)+(\partial u_{j+2,k+2}/\partial z)-(\partial u_{j-2,k+2}/\partial z)$$
$$-(\partial u_{j+2,k-2}/\partial z)]$$
$$- (4/9\Delta x\Delta z)[(\partial u_{j-1,k-1}/\partial z)+(\partial u_{j+1,k+1}/\partial z)-(\partial u_{j-1,k+1}/\partial z)$$
$$-(\partial u_{j+1,k-1}/\partial z)]\ , \qquad \text{(A-6)}$$

$$\partial^3 u_{j,k}/\partial x^2\partial z = (31/864\Delta x^2\Delta z)[u_{j+2,k+2} - u_{j-2,k-2} + u_{j-2,k+2} - u_{j+2,k-2}$$
$$+ 2u_{j,k-2} - 2u_{j,k+2}]$$
$$+ (44/27\Delta x^2\Delta z)[u_{j+1,k+1} - u_{j-1,k-1} + u_{j-1,k+1} - u_{j+1,k-1} + 2u_{j,k-1}$$
$$- 2u_{j,k+1}]$$
$$- (1/144\Delta x^2)[(\partial u_{j-2,k-2}/\partial z) + (\partial u_{j+2,k+2}/\partial z) + (\partial u_{j-2,k+2}/\partial z)$$
$$+ (\partial u_{j+2,k-2}/\partial z) - 2(\partial u_{j,k+2}/\partial z) - 2(\partial u_{j,k-2}/\partial z)]$$
$$- (4/9\Delta x^2)[(\partial u_{j-1,k-1}/\partial z)+(\partial u_{j+1,k+1}/\partial z)+(\partial u_{j-1,k+1}/\partial z)+(\partial u_{j+1,k-1}/\partial z)$$
$$- 2(\partial u_{j,k+1}/\partial z) - 2(\partial u_{j,k-1}/\partial z)]$$

$$- (1/144\Delta x\Delta z)[(\partial u_{j-2,k-2}/\partial x)+(\partial u_{j+2,k+2}/\partial x)-(\partial u_{j-2,k+2}/\partial x)$$
$$-(\partial u_{j+2,k-2}/\partial x)]$$
$$- (4/9\Delta x\Delta z)[(\partial u_{j-1,k-1}/\partial x)+(\partial u_{j+1,k+1}/\partial x)-(\partial u_{j-1,k+1}/\partial x)$$
$$-(\partial u_{j+1,k-1}/\partial x)] , \qquad \text{(A-7)}$$

where Δx, Δz denote the space increment in the x- and z-directions, respectively.

Similarly, the corresponding computational equations related to the particle-velocity v can be obtained simply by substituting u by v into (A-1) ~ (A-7).

APPENDIX B

DERIVATION OF STABILITY CRITERION

1D case

To derive the stability criterion of the ENAD-FRK method for the 1D acoustic case, we consider the harmonic solution of eq. (8). Substitute the harmonic solution

$$[u_j^n, (\partial u/\partial x)_j^n, v_j^n, (\partial v/\partial x)_j^n]^T$$
$$= [u^n, (\partial u^n/\partial x), v^n, (\partial v^n/\partial x)]^T \exp[i(\omega_{num} n\Delta t + kj\Delta x)] , \qquad \text{(B-1)}$$

into eq. (8) with the eighth-order derivatives, we can obtain the following equations

$$[u^{n+1}, (\partial u^{n+1}/\partial x), v^{n+1}, (\partial v^{n+1}/\partial x)]^T = \mathbf{H}[u^n, (\partial u^n/\partial x), v^n, (\partial v^n/\partial x)]^T , \qquad \text{(B-2)}$$

where the amplification matrix is defined by $\mathbf{H} = \begin{pmatrix} h_{11} & h_{12} & h_{13} & h_{14} \\ h_{21} & h_{22} & h_{23} & h_{24} \\ h_{31} & h_{32} & h_{33} & h_{34} \\ h_{41} & h_{42} & h_{43} & h_{44} \end{pmatrix}$.

The elements of the H are shown as follows

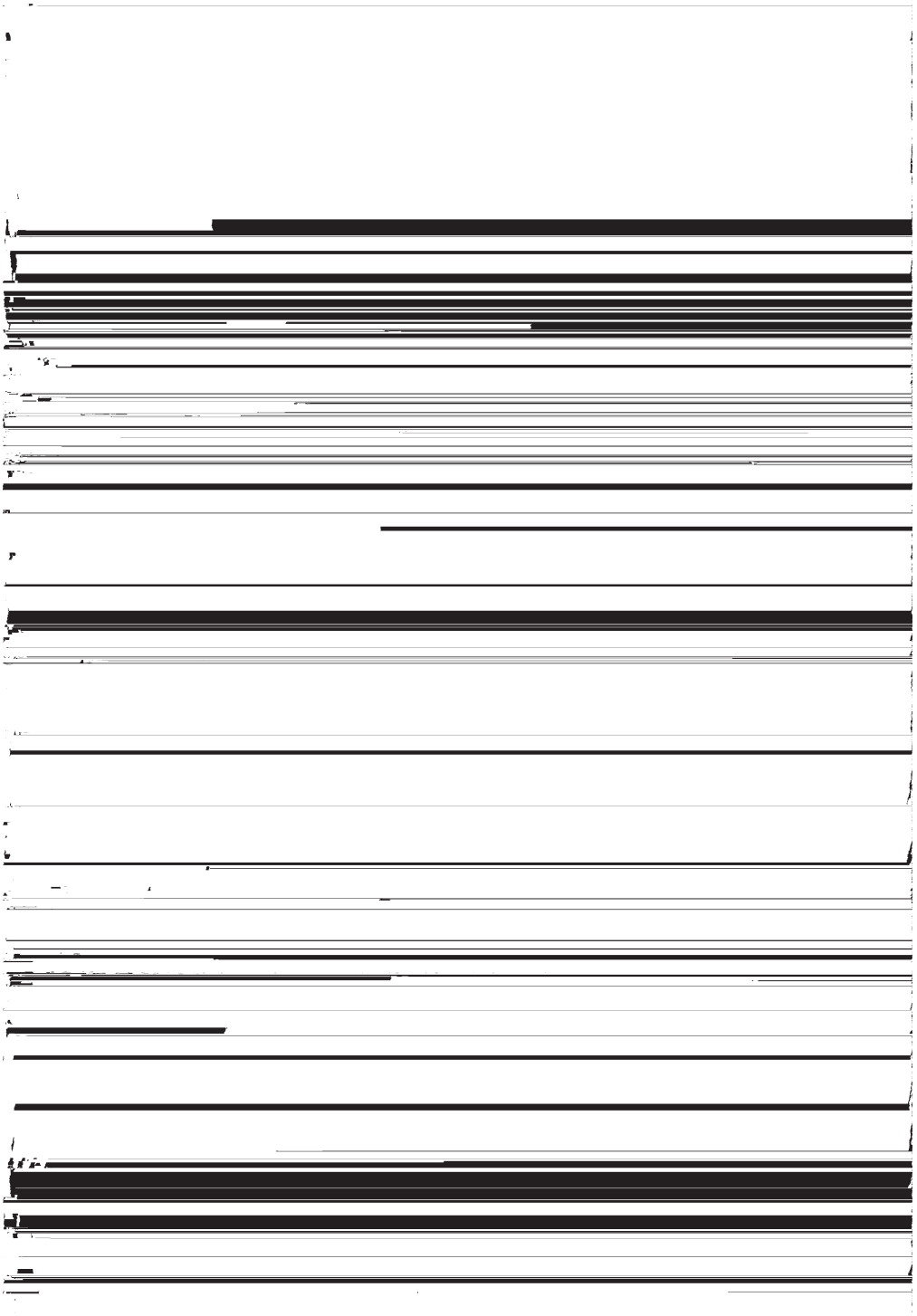

$$h_{41} = (i\alpha^2/ht)[(176/9)\sin\theta + (31/72)\sin 2\theta]$$
$$+ (i\alpha^4/ht)[-(95489/1458)\sin\theta - (7001/1458)\cos\theta\sin\theta$$
$$+ (43/162)\sin 3\theta + (589/93312)\sin 4\theta] ,$$
$$h_{42} = -(\alpha^2/t)[15 + (16/3)\cos\theta + (1/12)\cos 2\theta]$$
$$+ (\alpha^4/t)[(27715/648) + (4357/162)\cos\theta - (107/972)\cos 2\theta$$
$$- (13/162)\cos 3\theta - (11/7776)\cos 4\theta] ,$$

where $\alpha = c\Delta t/\Delta x$ denotes the Courant number, $\theta = k\Delta x$, $i = \sqrt{-1}$.

From the amplification matrix **H**, we can numerically obtain the following stability criterion of the ENAD-FRK method for the 1D case by solving the eigenvalue problem $|\lambda_l(\mathbf{H})| \leq 1$ for all eigenvalues $\lambda_l(\mathbf{H})$, $l = 1,2,3,4$,

$$\alpha \leq \alpha_{max} \approx 0.69313 , \tag{B-3}$$

where α_{max} denotes the maximum Courant number.

2D case

To obtain the stability condition of the ENAD-FRK method for the 2D acoustic case, for simplicity we consider the harmonic solution of eq. (8) under the condition $\Delta x = \Delta z = h$. Substituting the solution

$$U^n_{j,l} = U^n \exp\{i[\omega_{num} n\Delta t + k(j\Delta x\cos\theta + l\Delta z\sin\theta)]\} , \tag{B-4}$$

where

$$U^n_{j,l} = [u^n_{j,l}, (\partial u/\partial x)^n_{j,l}, (\partial u/\partial z)^n_{j,l}, v^n_{j,l}, (\partial v/\partial x)^n_{j,l}, (\partial v/\partial z)^n_{j,l}] ,$$
$$U^n = [u^n, (\partial u^n/\partial x), (\partial u^n/\partial z), v^n, (\partial v^n/\partial x), (\partial v^n/\partial z)] ,$$

into eq. (8) with relations (A-1) to (A-7), we can obtain the following equation

$$[u^{n+1},(\partial u^{n+1}/\partial x),(\partial u^{n+1}/\partial z),v^{n+1},(\partial v^{n+1}/\partial x)]^T$$
$$= \mathbf{G}[u^n,(\partial u^n/\partial x),(\partial u^n/\partial z),v^n,(\partial v^n/\partial x),(\partial v^n/\partial z)]^T . \tag{B-5}$$

Due to the complexity of the elements g_{ij} of the amplification matrix **G**, here we only show the first row of **G** as follows

$$g_{11} = 1 + [-5 + (64/27)\cos\xi + (7/54)\cos 2\xi + (64/27)\cos\eta + (7/54)\cos 2\eta]\alpha^2 + [(849925/139968) - (31775/8748)\cos\xi - (129059/559872)\cos 2\xi + (223/8748)\cos 3\xi + (299/279936)\cos 4\xi - (11/2916)\cos(\xi - 3\eta) - (31/11664)\cos(2\xi - 3\eta) - (2339/34992)\cos(\xi - 3\eta) - (31/373248)\cos(2\xi - 2\eta) - (31/11664)\cos(3\xi - 2\eta) - (31/373248)\cos(4\xi - 2\eta) + (4129/4374)\cos(\xi - \eta) + (49/17496)\cos 2(\xi - \eta) - (2339/34992)\cos(2\xi - \eta) - (11/2916)\cos(3\xi - \eta) - (31775/8748)\cos\eta - (129059/559872)\cos 2\eta + (223/8748)\cos 3\eta + (299/279936)\cos 4\eta + (4129/4374)\cos(\xi + \eta) + (49/17496)\cos(2\xi + 2\eta) - (2339/34992)\cos(2\xi + \eta) - (31/373248)\cos(4\xi + 2\eta) - (11/2916)\cos(3\xi + \eta) - (2339/34992)\cos(\xi + 2\eta) - (31/373248)\cos(2\xi + 4\eta) - (31/11664)\cos(3\xi + 2\eta) - (11/2916)\cos(\xi + 3\eta) - (31/11664)\cos(2\xi + 3\eta)]\alpha^4 ,$$

$$g_{12} = ih\alpha^2[-(8/9)\sin\xi - (1/18)\cos\xi\sin\xi] + ih\alpha^4[(871/486)\sin\xi + (1301/46656)\cos\xi\sin\xi - (13/1458)\sin 3\xi - (11/46656)\sin 4\xi + (1/972)\sin(\xi - 3\eta) + (1/1944)\sin(2\xi - 3\eta) + (133/5832)\sin(\xi - 2\eta) + (1/62208)\sin(2\xi - 4\eta) + (1/1944)\sin(3\xi - 2\eta) + (1/62208)\sin(4\xi - 2\eta) - (128/729)\sin(\xi - \eta) - (7/23328)\sin 2(\xi - \eta) + (157/5832)\sin(2\xi - \eta) + (1/972)\sin(3\xi - \eta)$$

$$- (128/729)\sin(\xi+\eta) - (7/23328)\sin2(\xi+\eta)$$

$$+ (157/5832)\sin(2\xi+\eta) + (1/62208)\sin(4\xi+2\eta)$$

$$+ (1/972)\sin(3\xi+\eta) + (133/5832)\sin(\xi+2\eta)$$

$$+ (1/62208)\sin(2\xi+4\eta) + (1/1944)\sin(3\xi+2\eta)$$

$$+ (1/972)\sin(\xi+3\eta) + (1/1944)\sin(2\xi+3\eta)] \quad ,$$

$$g_{13} = ih\alpha^2[-(8/9)\sin\eta - (1/18)\cos\eta\sin\eta] + ih\alpha^4[(-1/972)\sin(2\xi-\eta)$$

$$- (1/1944)\sin(2\xi-3\eta) - (133/5832)\sin(\xi-2\eta)$$

$$- (1/62208)\sin(2\xi-4\eta) - (1/1944)\sin(3\xi-2\eta)$$

$$- (1/62208)\sin(4\xi-2\eta) + (128/729)\sin(\xi-\eta)$$

$$+ (7/23328)\sin2(\xi-\eta) - (133/5832)\sin(2\xi-\eta)$$

$$- (1/972)\sin(3\xi-\eta) + (871/486)\sin\eta)$$

$$+ (1301/46656)\cos\eta\sin\eta - (13/1458)\sin3\eta$$

$$- (11/46656)\sin4\eta - (128/729)\sin(\xi+\eta)$$

$$- (7/23328)\sin2(\xi+\eta) + (133/5832)\sin(2\xi+\eta)$$

$$+ (1/62208)\sin(4\xi+2\eta) + (1/972)\sin(3\xi+\eta)$$

$$+ (157/5832)\sin(\xi+2\eta) + (1/62208)\sin(2\xi+4\eta)$$

$$+ (1/1944)\sin(3\xi+2\eta) + (1/972)\sin(\xi+3\eta)$$

$$+ (1/1944)\sin(2\xi+3\eta)] \quad ,$$

$$g_{14} = t + t\alpha^2[-(5/3) + (64/81)\cos\xi + (7/162)\cos2\xi$$

$$+ (64/81)\cos\eta + (7/162)\cos2\eta] \quad ,$$

$$g_{15} = ith\alpha2[-(8/27)\sin\xi - (1/54)\sin\xi\cos\xi] \quad ,$$

$$g_{16} = ith\alpha2[-(8/27)\sin\eta - (1/54)\sin\eta\cos\eta] \quad ,$$

where $\Delta x = \Delta z = h$, $\xi = kh\cos\theta$, $\eta = kh\sin\theta$, $\alpha = c_0\Delta t/h$, $i = \sqrt{-1}$. $k\cos\theta$

and ksinθ are the wave numbers, θ is the wave propagation angle with respect to the x-axis.

From the amplification matrix **G**, we can numerically obtain the following stability criterion of the ENAD-FRK method for the 2D case by solving the eigenvalue problem $|\lambda_l(\mathbf{G})| \leq 1$ for all eigenvalues $\lambda_l(\mathbf{G})$, $l = 1,2,\ldots,6$.

$$\alpha \leq \alpha_{max} \approx 0.69313 \quad , \tag{B-6}$$

where α_{max} denotes the maximum Courant number.

APPENDIX C

DERIVATION OF THE NUMERICAL DISPERSION RELATION

To obtain the numerical dispersion relation of the ENAD-FRK method for the 2D acoustic case, we consider the harmonic solution of eq. (8) while $\Delta x = \Delta z = h$ and substitute the solution

$$U^n_{j,l} = U^0 \exp\{i[\omega_{num} n\Delta t + j(kh\Delta x \cos\theta) + l(kh \sin\theta)]\} \quad , \tag{C-1}$$

where

$$U^n_{j,l} = [u^n_{j,l}, (\partial u/\partial x)^n_{j,l}, (\partial u/\partial z)^n_{j,l}, v^n_{j,l}, (\partial v/\partial x)^n_{j,l}, (\partial v/\partial z)^n_{j,l}] \quad ,$$

$$U^0 = [u^0, (\partial u^0/\partial x), (\partial u^0/\partial z), v^0, (\partial v^0/\partial x), (\partial v^0/\partial z)] \quad ,$$

into eq. (8) with relations (A-1) to (A-7) to obtain the following dispersion equation

$$\mathrm{Det}(e^{i\gamma} \mathbf{I}_6 - \mathbf{G}) = 0 \quad , \tag{C-2}$$

where $\gamma = \omega_{num}\Delta t$, $i = \sqrt{-1}$, **G** is the same as that presented in eq. (B-5) and $\mathbf{I}_6$ is a sixth-order identity matrix.

For convenience, we suppose $c_{num} = \omega_{num}/k$, $k = 2\pi/\lambda$, $\alpha = c\Delta t/h$, $S = h/\lambda$, $\xi = kh\cos\theta$, and $\eta = kh\sin\theta$. By solving the dispersion eq. (C-2), we can get the following ratio of the numerical velocity (c_{num}) to the exact velocity (c_0)

$$R = c_{num}/c_0 = \gamma/2\pi\alpha S \quad , \tag{C-3}$$

where γ satisfies eq. (C-2), which is a nonlinear function with respect to α and S.